lis-1 is required for dynein-dependent cell division processes in *C. elegans* embryos

Moira M. Cockell, Karine Baumer and Pierre Gönczy*

Swiss Institute for Experimental Cancer Research (ISREC), Ch. des Boveresses 155, 1066 Epalinges/Lausanne, Switzerland
*Author for correspondence (e-mail: pierre.gonczy@isrec.unil.ch)

Accepted 3 June 2004
Journal of Cell Science 117, 4571-4582 Published by The Company of Biologists 2004
doi:10.1242/jcs.01344

Summary

We investigated the role of the evolutionarily conserved protein Lis1 in cell division processes of *Caenorhabditis elegans* embryos. We identified apparent null alleles of *lis-1*, which result in defects identical to those observed after inactivation of the dynein heavy chain *dhc-1*, including defects in centrosome separation and spindle assembly. We raised antibodies against LIS-1 and generated transgenic animals expressing functional GFP–LIS-1. Using indirect immunofluorescence and spinning-disk confocal microscopy, we found that LIS-1 is present throughout the cytoplasm and is enriched in discrete subcellular locations, including the cell cortex, the vicinity of microtubule asters, the nuclear periphery and kinetochores. We established that *lis-1* contributes to, but is not essential for, DHC-1 enrichment at specific subcellular locations. Conversely, we found that *dhc-1*, as well as the dynactin components *dnc-1* (p150^{Glued}) and *dnc-2* (p50/dynamitin), are essential for LIS-1 targeting to the nuclear periphery, but not to the cell cortex nor to kinetochores. These results suggest that dynein and Lis1, albeit functioning in identical processes, are targeted partially independently of one another.

Movies and supplemental data available online

Key words: Lissencephaly, Cytoplasmic dynein, Spindle assembly, Centrosome separation

Introduction

Patients lacking one functional copy of the *Lis1* gene suffer from lissencephaly, a severe neurological disorder characterized by a lack of proliferation, migration and survival of cortical neurons during development (Gambello et al., 2003; Hattori et al., 1994; Reiner et al., 1993). Lis1 is a WD40-repeat-containing protein conserved from budding yeast to humans and is thought to participate in several cellular processes through its interaction with cytoplasmic dynein, the major minus-end-directed microtubule motor of eukaryotic cells (Faulkner et al., 2000; Geiser et al., 1997; Smith et al., 2000). However, it is still unclear whether Lis1 serves as an obligatory cofactor for all dynein-dependent processes or if it has dynein-independent functions.

The dynein complex contains multiple subunits, including a heavy chain dimer that provides ATP-dependent motor activity (reviewed by Holzbaur and Vallee, 1994). Moreover, coupling of motor activity to cargo requires interaction with the adaptor complex dynactin (Gill et al., 1991). Dynein is responsible for transporting a wide variety of cargoes towards the minus end of microtubules and is required for several cell division processes, including centrosome separation and spindle assembly (Gönczy et al., 1999a; Karki and Holzbaur, 1999; Vaisberg et al., 1993) (reviewed by Vale, 2003). As expected from such multiple roles, dynein is distributed throughout the cytoplasm, but is also enriched at discrete subcellular locations, including the cell cortex, the nuclear periphery and kinetochores (Busson et al., 1998; Gönczy et al., 1999a; King et al., 2000; Lin and Collins, 1992; Pfarr et al., 1990; Steuer et al., 1990). Whereas the distribution of Lis1 often overlaps with that of dynein, co-immunoprecipitation studies indicate that only a fraction of dynein and Lis1 are associated in vivo (Aumais et al., 2001; Coquelle et al., 2002; Faulkner et al., 2000; Smith et al., 2000; Tai et al., 2002), raising the possibility that the two proteins are targeted independently of one another to some specific subcellular locations.

Dynein anchored at the cell cortex has been implicated in governing centrosome and spindle positioning by reeling in the plus end of microtubules (reviewed by Dujardin and Vallee, 2002; Gönczy, 2002; Xiang, 2003). Lis1 might contribute to this aspect of dynein function because budding yeast cells lacking the Lis1 homologue Pac1p fail to undergo dynein-mediated interactions between microtubule plus ends and the cortex (Sheeman et al., 2003). Microtubules are longer on average due principally to a lowered frequency of catastrophes in mutants of the *A. nidulans* Lis1 homologue *nudF*, as well as in mutants of the dynein heavy chain gene *nudA* (Han et al., 2001), raising the possibility that Lis1 and dynein act by modulating microtubule dynamics. NudF is enriched at the plus end of microtubules in *A. nidulans* (Han et al., 2001), as is Pac1p in *Saccharomyces cerevisiae* (Lee et al., 2003). Interestingly, Pac1p interacts genetically and physically with Bik1p, a microtubule plus-end-associated protein of the CLIP-170 family (Lee et al., 2003; Sheeman et al., 2003) and overexpression of mammalian CLIP-170 recruits a phosphorylated Lis1 isoform to microtubules (Coquelle et al., 2002). Therefore, although Lis1 is found throughout microtubule-dense areas in mammalian cells (Aumais et al., 2001; Smith et al., 2000), it has been proposed that Lis1 plays an evolutionarily conserved role at microtubule plus ends (reviewed by Dujardin and Vallee, 2002).

Dynein anchored at the nuclear periphery is thought to generate tension on the nuclear envelope that triggers nuclear envelope breakdown (NEBD) (Beaudouin et al., 2002; Salina et al., 2002). Although dynein promotes efficient NEBD, it is not absolutely required for this process, which can also occur via an alternative, microtubule-independent pathway (Beaudouin et al., 2002; Salina et al., 2002). Lis1 is present at the nuclear periphery of HeLa cells (Coquelle et al., 2002), but whether its presence at that subcellular location requires dynein function is not known.

Kinetochore-associated dynein has been proposed to contribute to poleward movement of chromosomes during prometaphase and anaphase in *Drosophila* (Savoian et al., 2000; Sharp et al., 2000). Lis1 is also enriched at kinetochores during prometaphase in polarized epithelial cells, and microinjection of anti-Lis1 antibodies or Lis1 overexpression both lead to chromosome segregation defects, suggesting that Lis1 is essential for dynein function at kinetochores (Faulkner et al., 2000). Overexpression of the dynactin subunit p50 disrupts kinetochore association of both dynein and Lis1, whereas overexpression of N-terminal Lis1 fragments displaces endogenous Lis1, but not dynein, from kinetochores (Coquelle et al., 2002; Tai et al., 2002). These observations have led these authors to suggest that dynein is required for Lis1 recruitment or maintenance at kinetochores. Whether a similar conclusion would be reached using loss-of-function analysis has not been addressed until now.

Because of its genetic tractability and potential for high-resolution cellular analysis, the early *C. elegans* embryo provides an excellent opportunity to dissect the in vivo requirement of dynein and Lis1 in a metazoan organism. Inactivation of *dhc-1* using RNA interference (RNAi) results in characteristic cell division defects in one-cell-stage embryos, including in pronuclear migration, centrosome separation and spindle assembly (Gönczy et al., 1999a). DHC-1 is present throughout the cytoplasm, but is also enriched at the cell cortex, in the vicinity of microtubule asters, at the nuclear periphery and at kinetochores (Gönczy et al., 1999a). Suggestively, pronuclear migration and spindle assembly are also defective in *lis-1*(*RNAi*) one-cell-stage embryos (Dawe et al., 2001; Gönczy et al., 2000). However, these studies did not provide a detailed phenotypic analysis, or report on either the subcellular distribution of LIS-1 or the relationship between *lis-1* and *dhc-1*.

We have identified probable null alleles of *C. elegans lis-1* and have established that *lis-1* is required for all known dynein-mediated processes in one-cell-stage embryos, including pronuclear migration, centrosome separation and spindle assembly, as well as dynein-mediated transport of yolk granule cargo. We raised antibodies against LIS-1 and generated animals expressing a green fluorescent protein (GFP)–LIS-1 fusion that rescues *lis-1* mutant embryos to viability. We found that LIS-1 localizes throughout the cytoplasm and is enriched in discrete subcellular locations, including the cell cortex, the vicinity of microtubule asters, the nuclear periphery and kinetochores. Furthermore, we established that *lis-1* contributes to DHC-1 enrichment at specific subcellular locations. Conversely, we found that *dhc-1*, *dnc-1* and *dnc-2* contribute to LIS-1 enrichment at the cell cortex, are essential for LIS-1 targeting to the nuclear periphery, and appear dispensable for the presence of LIS-1 at kinetochores.

Materials and Methods

Nematode strains

Culturing of *C. elegans* was according to standard procedures (Brenner, 1974). Generation of *lis-1* mutant strains is described in detail elsewhere (Gönczy et al., 1999b). *lis-1* mutant strains were of genotypes *unc-32*(*e189*) *lis-1*(*t1550*) and *unc-32*(*e189*) *lis-1*(*t1698*), balanced by *qC1* [*dpy-19*(*e1259ts*) *glp-1*(*q339*)], and were left at 25°C for >12 hours before analysis. Transgenic animals expressing GFP-β-tubulin (GFP-TUB) and GFP-histone2B (GFP-HIS) have been described (Strome et al., 2001).

We found that *unc-32*(*e189*) *lis-1*(*t1550*)/*unc-32*(*e189*) *lis-1*(*t1698*) animals yielded embryos with an identical phenotype to that of embryos derived from either homozygous mutant strain. We noted that *lis-1*(*t1550*) and *lis-1*(*t1698*) heterozygote animals give rise to ~75% of the expected frequency of homozygous mutant progeny, indicating a partial zygotic requirement for viability. We noted also that the brood size of homozygous *lis-1(t1550) and (t1698)* animals at 20°C is ~50 (wild-type ~200), whereas that of animals fed with *dhc-1(RNAi)* for 24 hours at 20°C is ~150. Homozygous *lis-1(t1550)* or *lis-1(t1698)* animals subjected to *dhc-1(RNAi)* for 24 hours are essentially sterile, establishing that *lis-1* and *dhc-1* genetically interact during oogenesis.

Characterization of *lis-1* mutations

Several independent reverse transcriptase polymerase chain reactions (RT-PCRs) of the *lis-1* gene (the sequence of these and all other primers are available upon request) were carried out, using poly A^+ RNA from wild-type and homozygous mutant adults as template (OneStep RT-PCR and RNAeasy kits, Quiagen). The resulting fragments were cloned and sequenced. A 1.9 kb genomic fragment starting at the first ATG of the *lis-1* gene up to the beginning of exon 5 was also amplified in several independent reactions and sequenced. The mutation in allele *t1550* results in a premature stop codon at amino acid 92, whereas that in allele *t1698* alters the splice acceptor of exon 4, usually generating a product of 128 amino acids that diverges from the LIS-1 sequence after amino acid 84. These mutations were found in all independent reactions examined.

GFP–LIS-1 transgenic animals

Sequence-verified full-length *lis-1* cDNA was subcloned into pSU25, a modified version of the *pie1-gfp* vector carrying an *unc-119* cDNA (kindly provided by Michael Glotzer), and bombarded essentially as described (Praitis et al., 2001). We obtained four independent non-integrated transgenic lines, which transmitted the extrachromosomal array to 40-70% of their progeny. The distribution of GFP was similar in all lines showing expression, albeit with significant differences in level.

To test for rescue, males carrying the GFP–LIS-1 extrachromosomal array (strain GZ 410**)** were mated with *unc-32 lis-1(t1550)/qC1* hermaphrodites, and the F1 progeny backcrossed to *unc-32 lis-1(t1550)/qC1* to generate F2 progeny with the genotype *unc-32 lis-1(t1550)qC1*;exGFP–LIS-1. F3 Unc animals were singled and allowed to lay embryos, whose viability was assessed. Approximately 70% of Unc animals gave rise to viable progeny. All Unc animals that gave rise to viable progeny expressed the GFP–LIS-1 transgene (n>60), whereas all Unc animals that did not give rise to viable progeny failed to express GFP–LIS-1 (n>30). 82% of embryos (n=397 embryos) laid by Unc animals expressing GFP–LIS-1 (n=14 worms) survived to adulthood, with the remaining 18% dying perhaps due to transgene loss during embryogenesis or inappropriate expression levels.

RNAi feeding bacteria

RNAi feeding strains were generated and dispensed essentially as

described (Kamath et al., 2001). The following fragments were obtained using PCR and cloned into L4440 (Timmons et al., 2001): *lis-1*, full-length cDNA; *dhc-1*, 1.3 kb cDNA C-terminal fragment derived from yk161f11; *dnc-1*, a ~1.5 kb genomic piece (positions 18546 to 20026 on cosmid ZK593); and *dnc-2*, ~1.1 kb genomic piece (positions 41973 to 43110 on cosmid C28H8). The *icp-1* and *tba-2* RNAi feeding strains were gifts from Michael Glotzer. The duration of feeding required to obtain strong phenotypes at 20°C was determined to be as follows: *lis-1* 30-40 hours; *dhc-1* 24-30 hours; *dnc-1* 35-45 hours; *dnc-2* 35-45 hours; *icp-1* 24-30 hours; *tba-2* 22-26 hours. Since the *hcp-4* RNAi feeding strain did not result in the previously reported strong phenotype (Oegema et al., 2001), we inactivated *hcp-4* by targeting a 1.5 kb genomic fragment (Oegema et al., 2001) using RNAi by injection essentially as described (Gönczy et al., 2000).

Time-lapse microscopy

Embryos were analysed by time-lapse DIC microscopy at 23±1°C, capturing 1 image every 5 seconds. Analysis of yolk granule velocities was conducted as described (Gönczy et al., 1999a), recording in the interval between NEBD and anaphase at 1 frame every 0.5 second and selecting yolk granules that could be followed for a minimum of 5 consecutive frames.

Spinning-disc time-lapse confocal microscopy was performed essentially as described (Bellanger and Gönczy, 2003), capturing 1 image every 10 seconds. For Fig. 5D and corresponding movie 16, imaging was on a Zeiss LSM 510 confocal microscope with appropriate settings. Fluorescence recovery after photobleaching (FRAP) experiments were performed on the Zeiss LSM510 confocal microscope, bleaching the area of interest with 20 iterations and 100% laser power, and monitoring fluorescence recovery in one ~1 μm confocal slice every 10 seconds thereafter. FITC-labelled 70 kDa Dextran (a gift from Joël Beaudouin and Jan Ellenberg) was injected into the gonad of a young wild-type adult and the resulting embryos analysed ~5 hours thereafter.

Antibodies and immunofluorescence

We generated purified recombinant protein containing 6 histidine residues fused to LIS-1 amino acids 1-141, which was injected into a rabbit (Eurogentec). The third bleed serum was purified against recombinant GST–LIS-1(1-141) coupled to CnBr-activated Sepharose 4B (Amersham Pharmacia Biotech AB). Bound antibodies were eluted with 100 mM glycine pH2, neutralized, dialysed against PBS and kept in 50% glycerol.

Embryos were fixed and stained essentially as described (Gönczy et al., 1999a). Primary antibodies were 1:400 mouse anti-α-tubulin (DM1A; Sigma), 1:6000 rabbit anti-ZYG-9 (Gönczy et al., 2001), 1:1000 rabbit anti-HCP-4 (Oegema et al., 2001), 1:1000 rabbit anti-ICP-1 (Oegema et al., 2001), 1:1000 rabbit anti-BUB-1 (Oegema et al., 2001), 1:150 or 1:300 rabbit anti-DHC-1 (Gönczy et al., 1999a), 1:300 rabbit anti-GFP (a gift from Viesturs Simanis), 1:1000 mouse anti-GFP **(**Chemicon**)**, 1:200 rabbit anti-LIS-1 (this study). Secondary antibodies were 1:2000 goat anti-mouse Alexa488 (Molecular Probes) or 1:1000 donkey anti-mouse Cy5 (Amersham), 1:300 goat anti-rabbit Alexa488 (Molecular Probes) or 1:2000 donkey anti-rabbit Cy3 (Dianova). Slides were counterstained with Hoechst 33258 (Sigma) to reveal DNA. Immunofluorescence data was acquired on a Zeiss LSM 510 confocal microscope. Images were processed with Adobe Photoshop.

Worm protein extracts and western blotting

Embryonic extracts from wild-type and *lis-1*(*RNAi*) were prepared by axenizing synchronized worm cultures according to standard procedures and resuspending a ~150 μl embryo pellet in 300 μl of 2× loading buffer. All extracts were homogenized for 20 seconds using a motorized pestle and boiled for 5 minutes prior to freezing.

Frozen extracts were reboiled for 1 minute before loading onto SDS-PAGE gels. Approximately 30 μl of each extract was loaded per lane on a 12.5% SDS acrylamide gel, run and transferred onto nitrocellulose. Filters were blocked for 15 minutes in TEN (10 mM Tris pH 7.5, 0.2 mM EDTA, 50 mM NaCl) + 5% milk, incubated overnight at 4°C with primary antibodies (1:1000) and the signal revealed with standard chemiluminesence (Amersham Pharmacia Biotech).

Quantitation of anti-LIS-1 reactivity in embryos

Early (i.e. <30 nuclei) wild-type embryos and *lis-1(RNAi)*, *lis-1(t1550)* or *lis-1(t1698)* embryos at the approximate equivalent stages and from the same slide were examined for anti-tubulin reactivity to identify those embryos that had undergone robust fixation and staining. Anti-LIS-1 reactivity in these embryos was then imaged using a 12-bit Spot RT Monochrome CCD camera (Diagnostic Instruments). The mean pixel intensity for a 100 μm^2 square within each embryo was determined using MetaMorph software (Universal Imaging) and expressed as a percentage of the average staining intensity of wild-type embryos on the same slide; 5-8 embryos of each type were examined per slide.

Results

Identification of probable null alleles of *C. elegans lis-1*

In a screen of maternal-effect embryonic lethal mutations, we identified two alleles of a gene called *pnm-1* that is essential for pronuclear migration (Gönczy et al., 1999b). Because this locus maps to the same chromosomal region as *lis-1* and because pronuclear migration is defective in *lis-1*(*RNAi*) embryos (Dawe et al., 2001; Gönczy et al., 2000), we sequenced the *lis-1* gene in the two *pnm-1* alleles. In both cases, we found a mutation predicted to significantly truncate LIS-1 (Materials and Methods). Moreover, expression of GFP–LIS-1 rescues the maternal-embryonic lethality of *pnm-1* mutant animals (see below). We conclude that *pnm-1* and *lis-1* are one and the same, and refer to this gene as *lis-1* from here on.

We raised polyclonal antibodies against LIS-1 that recognize a unique ~45 kDa band in embryonic extracts from wild-type worms, which is absent from *lis-1*(*RNAi*), *lis-1*(*t1550*) and *lis-1*(*t1698*) animals (Fig. 1A and data not shown). Moreover, the signal detected with these antibodies upon immunostaining of wild-type embryos is essentially absent in *lis-1(RNAi)*, *lis-1*(*t1550*) and *lis-1*(*t1698*) embryos (Fig. 1B,C). The lack of LIS-1 protein in the two alleles presumably stems from degradation of mutant mRNAs harbouring premature stop codons by nonsense-mediated decay (reviewed by Culbertson and Leeds, 2003). We found that RNAi-mediated inactivation of *lis-1* does not worsen the phenotype of *lis-1*(*t1550*) or *lis-1*(*t1698*) mutant embryos (data not shown). Taken together, these observations indicate that *t1550* and *t1698* are likely null alleles of *lis-1*.

lis-1 is required for dynein-mediated processes in one-cell-stage *C. elegans* embryos

We analysed one-cell-stage embryos lacking *lis-1* using time-lapse differential interference contrast (DIC) microscopy. In wild-type (Fig. 2A; Table 1; Movie 1, in supplementary material, http://jcs.biologists.org/cgi/content/full/117/19/4571/

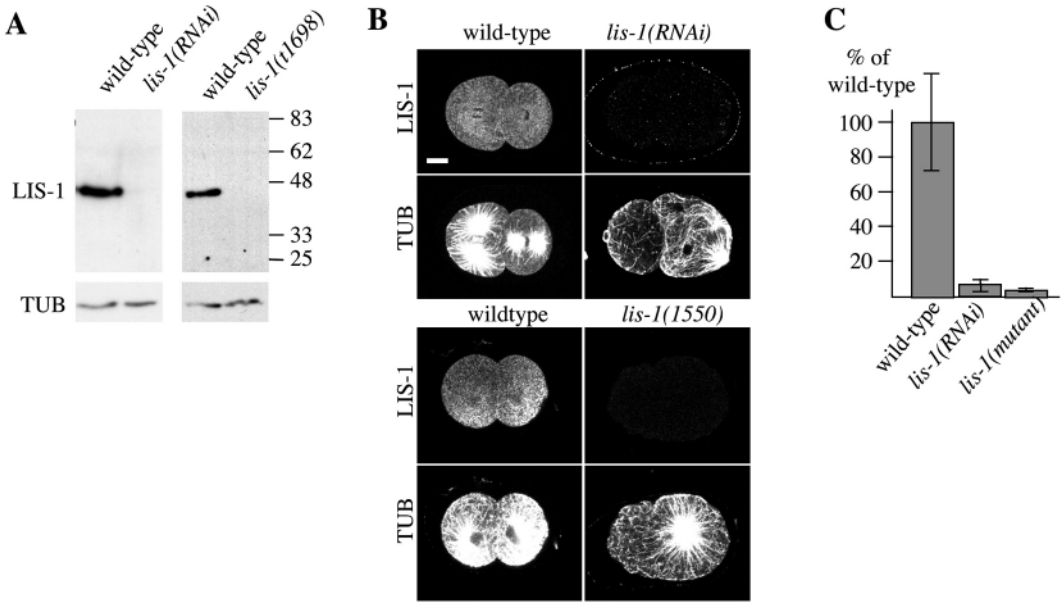

Fig. 1. Characterization of LIS-1 antibodies. (A) Western blots of protein extracts from wild-type, *lis-1(RNAi)* and *lis-1(t1698)* embryos, probed with LIS-1 antibodies and reprobed with α-tubulin (TUB) antibodies. We detected a ~15 kDa band in some extracts from mixed developmental stages of homozygote *lis-1(t1698)* mutant animals (not shown). (B) Wild-type, *lis-1(RNAi)* and *lis-1(t1550)* embryos stained with LIS-1 and α-tubulin antibodies. Wild-type embryos fixed and stained on the same slides as *lis-1(RNAi)* or *lis-1(t1550)* embryos are shown. Bar, 10 μm. (C) Quantification of average LIS-1 reactivity, expressed as a fraction of wild-type values for wild-type (100%, *n*=18), *lis-1(RNAi)* (5.2%; *n*=9) and *lis-1(t1550)* or *lis-1*(*t1698*) [referred to collectively as *lis-1*(*mutant*)] (2.9%; *n*=11) embryos.

DC1), the male pronucleus forms in close proximity to the posterior cortex, the female pronucleus on the opposite side (Fig. 2A, 00:00). The two centrosomes that are associated with the male pronucleus at this stage become apparent as small yolk-granule-depleted regions separating around the surface of the nuclear envelope, while moving away from the posterior cortex. Migration of the male and female pronuclei ensues. After meeting in the posterior half (Fig. 2A, 01:40), the two pronuclei and associated centrosomes move to the cell centrer while undergoing a 90° rotation, which is followed by NEBD and bipolar spindle assembly (Fig. 2A, 06:50). In *lis-1* mutant embryos (Fig. 2B; Table 1; Movie 2, in supplementary material) and *lis-1*(*RNAi*) embryos (Fig. 2C; Table 1; Movie 3, in supplementary material), the male and female pronuclei form in the correct locations (Fig. 2B,C, 00:00). However, in contrast to wild-type, the small yolk-granule-depleted regions do not separate around the surface of the nuclear envelope, but instead remain at the posterior cortex. Moreover, migration of the male and female pronuclei does not take place, and a bipolar spindle does not assemble (Fig. 2B, 05:20; Fig. 2C, 05:35). We also noted a yolk-granule-depleted region emanating from the centrosomes and extending towards the anterior of the embryo following breakdown of the male pronuclear envelope (Fig. 2B,C, arrows).

The above observations suggested that centrosomes fail to separate and to move away from the posterior cortex in the absence of *lis-1* function. This conclusion was verified by staining embryos with antibodies against the centrosomal component ZYG-9 (Matthews et al., 1998) (Fig. 2E, compare with Fig. 2D, arrowheads) as well as measuring centrosome-to-centrosome distance in live embryos expressing GFP-TUB (Fig. 2H). Staining of *lis-1* mutant embryos also revealed that the yolk-granule-depleted region observed in the time-lapse recordings corresponds to microtubules emanating from the two centrosomes (Fig. 2E, arrow). We also found that embryos at later stages often exhibit multiple closely juxtaposed centrosomes, indicating that they do not separate even after several rounds of duplication (Fig. 2G, compare with 2F). Overall, we conclude that *lis-1* is essential for centrosome separation, pronuclear migration and spindle assembly in *C. elegans* one-cell-stage embryos.

These processes also require the function of *dhc-1*, as well as of the dynactin components *dnc-1* and *dnc-2* (Gönczy et al., 1999a), suggesting that *lis-1* is generally required for dynein-mediated cell division processes. Compatible with this view, we observed three additional phenotypic traits in one-cell-stage embryos following *lis-1* inactivation that have been reported with *dhc-1*(RNAi) (Gönczy et al., 1999a). First, some *lis-1* mutant embryos have two or more female pronuclei, albeit at a lower frequency than *dhc-1(RNAi)* embryos (Table 1). Second, a fraction of *lis-1*(*RNAi*) embryos (19%; *n*=21) exhibit loss of association between centrosomes and male pronucleus. Third, partial inactivation of *lis-1* with RNAi leads to defective spindle orientation (data not shown). In summary, *lis-1* and dynein are required for essentially the same cell division processes in one-cell-stage *C. elegans* embryos.

To test whether *lis-1* is required more broadly for dynein-dependent function, we examined the occurrence of minus-end-directed movements of yolk granules (Materials and Methods). In the wild-type, these movements occur at an average velocity of ~1.5 μm/second and are driven by cytoplasmic dynein, thus providing a sensitive in vivo assay of dynein-dependent motility events (Gönczy et al., 1999a). As illustrated in Movies 4-7 (supplementary material,

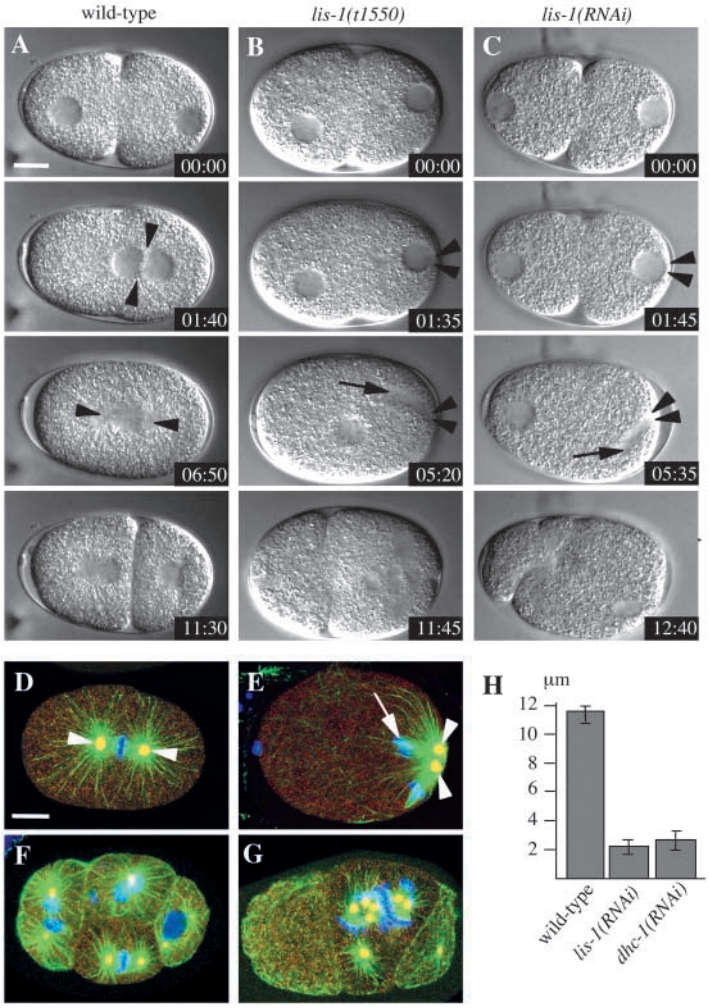

Fig. 2. *lis-1* is required for pronuclear migration, centrosome separation and bipolar spindle assembly. (A-C) Images from time-lapse DIC microscopy of wild-type (A), *lis-1(t1550)* (B) and *lis-1(RNAi)* (C) one-cell-stage embryos (see also corresponding Movies 1-3, in supplementary material, http://jcs.biologists.org/cgi/content/full/117/19/4571/DC1). In this and other figures, anterior is to the left, posterior to the right, bars represent 10 µm, and all panels of a kind are at approximately the same magnification, unless stated otherwise. Time elapsed is shown in minutes and seconds, with 00:00 corresponding to the time of maximal pseudocleavage furrow ingression. Arrowheads indicate the position of centrosomes as inferred primarily from fluorescence imaging of equivalent embryos expressing GFP-TUB. Arrows indicate anterior-most boundary of a region depleted of yolk granules that emanates from the centrosomes and extends towards the anterior following breakdown of the male pronuclear envelope. Note that breakdown of the male pronucleus precedes that of the female pronucleus as is generally the case when the two pronuclei are not juxtaposed (Gönczy et al., 1999a). Note also that furrowing initiates but does not go to completion towards the cell anterior in *lis-1*(*t1550*) and *lis-1*(*RNAi*) embryos, presumably reflecting a local minimum of microtubule density (Dechant and Glotzer, 2003). (D-G) Wild-type one-cell-stage embryo during metaphase (D) and *lis-1(t1550)* embryo at equivalent stage (E), as well as wild-type four-cell-stage embryo (F) and *lis-1(t1550)* embryo at equivalent stage (G) stained with antibodies against ZYG-9 (red) and α-tubulin (green) and counterstained with Hoechst to view DNA (blue). Yellow spots are indicative of ZYG-9 staining at centrosomes (arrowheads). Arrow indicates anterior-most boundary of microtubules emanating from the centrosomes and abutting chromosomes from the male gamete [see also Movie 16 (supplementary material) for similar feature in *dhc-1*(*RNAi*) embryo]. Images are projections of two consecutive 1 µm confocal slices. (H) Mean centrosome-to-centrosome distance, measured in live embryos expressing GFP-TUB, in wild-type (*n*=7), *lis-1(RNAi)* (*n*=15) and *dhc-1(RNAi)* (*n*=12) embryos at the time of male pronuclear envelope breakdown. Bars represent s.d.

http://jcs.biologists.org/cgi/content/full/117/19/4571/DC1), we found that minus-end-directed movements of yolk granules are essentially abolished when *lis-1* is inactivated, demonstrating that *lis-1* is also required for dynein-dependent cargo transport in vivo.

Subcellular distribution of LIS-1

We next sought to determine the subcellular distribution of LIS-1 in early embryos using indirect immunofluorescence.

Table 1. DIC phenotypes of one-cell-stage embryos with compromised *lis-1* or *dhc-1* function

Condition	Number of embryos	% Multiple female pronuclei (PN)	% PN migration*, bipolar spindle
Wild type	20	0	100
lis-1(*t1550*)	12	8	0
lis-1(*t1698*)	13	31	0
lis-1(*RNAi*)	17	12	0
dhc-1(*RNAi*)†	20	60	0

*Pronuclear migration refers to full-fledged movement of both male and female PN; minor movements of female PN towards the posterior are occasionally observed in embryos lacking *lis-1* or *dhc-1* function.
†*dhc-1*(*RNAi*) data is from Gönczy et al., 1999.

We found that LIS-1 is present throughout the cytoplasm, but is also enriched in discrete subcellular locations (Fig. 3A-I). In early one-cell-stage embryos, LIS-1 is typically detected within pronuclei during late prophase (Fig. 3B), before NEBD would be apparent by DIC microscopy (Fig. 1A, 01:40). In favourable specimens, LIS-1 can also be detected at the nuclear periphery during late prophase (Fig. 3G, arrowhead; two-cell-stage embryo) as well as in the vicinity of chromosomes during prometaphase (Fig. 3C,H, arrows). LIS-1 is depleted from the centres of microtubule asters during prometaphase (Fig. 3C, arrowheads), whereas it is enriched throughout the spindle during metaphase and early anaphase (Fig. 3E, arrowhead; two-cell-stage embryo). During late anaphase and telophase, LIS-1 staining diminishes on the spindle but becomes enriched in the vicinity of the microtubule asters (Fig. 3D, arrowheads, compare squares 1 and 2). Moreover, LIS-1 enrichment becomes apparent at the cell cortex at this stage (Fig. 3D, arrow). The discrete subcellular distributions of LIS-1 are typically more readily detectable in subsequent cell cycles. This is especially true of the nuclear enrichment in prophase (Fig. 3F, arrowheads), of the spindle enrichment in metaphase (Fig. 3E, arrowhead) and of the cortical localization (Fig. 3E, arrow).

To investigate which segments of microtubules colocalize

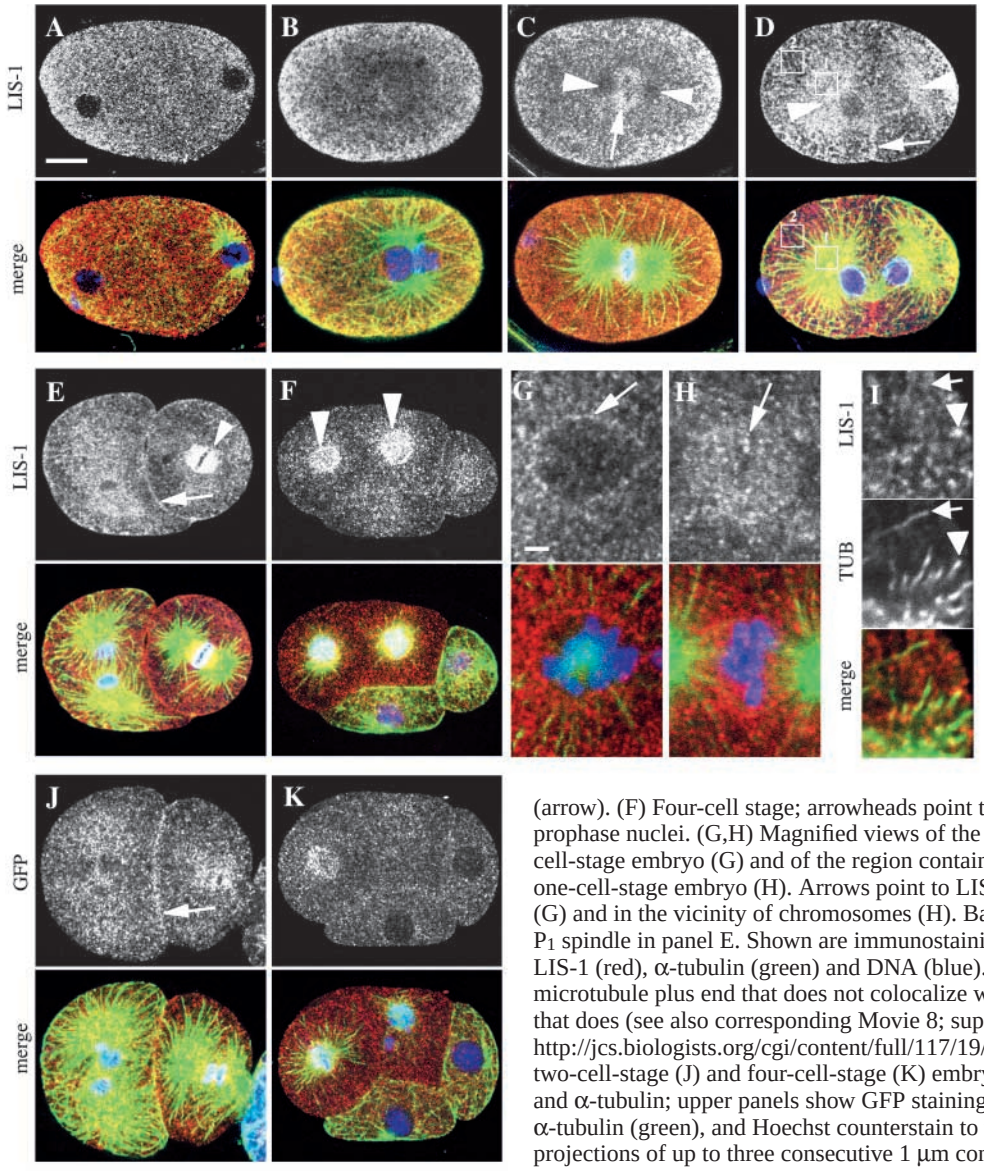

Fig. 3. LIS-1 distribution in early embryos. (A-I) Wild-type embryos stained with antibodies against LIS-1 and α-tubulin; upper panels show LIS-1 staining, lower panels the merge of LIS-1 (red), α-tubulin (green), and Hoechst counterstain to view DNA (blue). Bar, 10 μm. (A-D) One-cell stage. (A) Early prophase; LIS-1 is excluded from pronuclei. (B) Pronuclear meeting; LIS-1 is no longer excluded from pronuclei. (C) Late prometaphase; arrow points to enriched LIS-1 in the vicinity of chromosomes, arrowheads to LIS-1 depletion at the aster centres. (D) Telophase; arrow indicates LIS-1 enrichment at the ingressing central cortex, arrowheads regions of LIS-1 enrichment in the vicinity of microtubule asters. Square 1 indicates an area of high microtubule density, square 2 an area of low microtubule density. Note that LIS-1 staining is more intense in square 1. (E) Two-cell stage; note enrichment of LIS-1 on the P_1 spindle (arrowhead) and the cell cortex between AB and P_1 (arrow). (F) Four-cell stage; arrowheads point to LIS-1 enrichment in ABa and ABp prophase nuclei. (G,H) Magnified views of the nucleus in the AB blastomere of a two-cell-stage embryo (G) and of the region containing chromosomes in a prometaphase one-cell-stage embryo (H). Arrows point to LIS-1 enrichment at the nuclear periphery (G) and in the vicinity of chromosomes (H). Bar, 2 μm. (I) Three-fold magnification of P_1 spindle in panel E. Shown are immunostaining of LIS-1, α-tubulin and the merge of LIS-1 (red), α-tubulin (green) and DNA (blue). Arrow points to an apparent microtubule plus end that does not colocalize with a focus of LIS-1, arrowhead to one that does (see also corresponding Movie 8; supplementary material, http://jcs.biologists.org/cgi/content/full/117/19/4571/DC1). (J,K) GFP–LIS-1 transgenic two-cell-stage (J) and four-cell-stage (K) embryos stained with antibodies against GFP and α-tubulin; upper panels show GFP staining, lower panels the merge of GFP (red), α-tubulin (green), and Hoechst counterstain to view DNA (blue). Images are projections of up to three consecutive 1 μm confocal slices.

with LIS-1, we examined embryos stained with LIS-1 antibodies at higher resolution (Fig. 3I; Movie 8, in supplementary material, http://jcs.biologists.org/cgi/content/full/117/19/4571/DC1). We found that whereas foci of LIS-1 colocalize with the plus end of some astral microtubules (Fig. 3I, arrowhead), this is not always the case (Fig. 3I, arrow), and many LIS-1 foci are found throughout the microtubule lattice (Fig. 3D,E; Movie 8, in supplementary material). Therefore, *C. elegans* LIS-1 is not detected strictly at the plus end of microtubules.

LIS-1 dynamics in *C. elegans* embryos

To examine the subcellular distribution of LIS-1 in living cells, we generated transgenic lines expressing GFP–LIS-1 under the control of a germline promoter. We found that the transgene rescues *lis-1*(*t1550*) mutant embryos to viability, establishing that the fusion protein is functional (Materials and Methods). Moreover, immunostaining of embryos expressing GFP–LIS-1 using GFP antibodies showed an analogous distribution to that of endogenous LIS-1 as detected by LIS-1 antibodies (Fig. 3J,K, compare with 3E,F).

We imaged embryos expressing GFP–LIS-1 using spinning-disc confocal time-lapse fluorescence microscopy (Movies 9 and 10, in supplementary material). This allowed us to observe with particular clarity the accumulation at the nuclear periphery during late prophase (Fig. 4A, 01:55 and 03:50), as well as the enrichment along chromosomes during prometaphase (Fig. 4A, 05:40; Fig. 5A).

Furthermore, imaging of GFP–LIS-1 allowed us to investigate in more detail the nuclear accumulation that occurs during prophase prior to apparent NEBD (Fig. 4A, 03:50 and Fig. 4B, 02:15). Quantification of signal intensities in four-cell-stage embryos shows a ~2.5-fold increase in nuclear GFP–LIS-1 during the ~120 seconds preceding NEBD (Fig. 4C). As expected, this nuclear increase is accompanied by a slight decrease of overall cytoplasmic signal intensity (Fig. 4C). The rapid nature of these alterations raised the possibility that

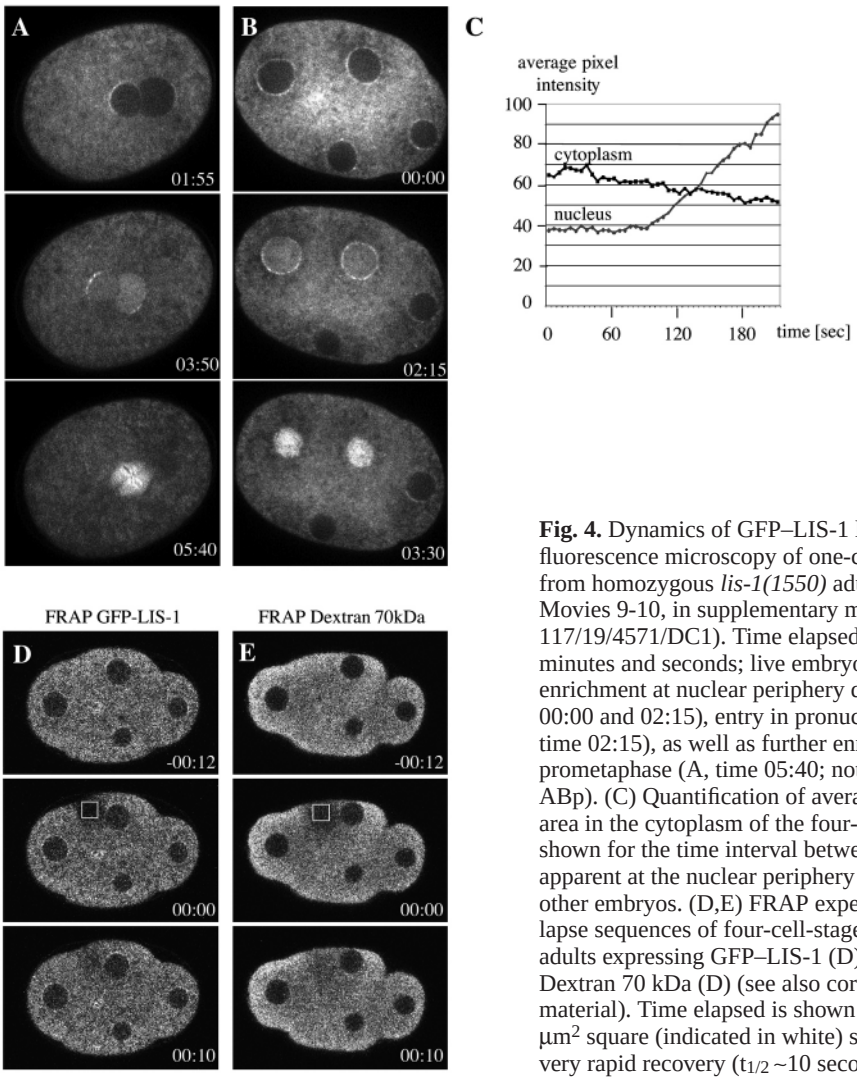

Fig. 4. Dynamics of GFP–LIS-1 localization. (A,B) Spinning-disc confocal time-lapse fluorescence microscopy of one-cell-stage (A) and four-cell-stage (B) embryos derived from homozygous *lis-1(1550)* adults expressing GFP–LIS-1 (see also corresponding Movies 9-10, in supplementary material, http://jcs.biologists.org/cgi/content/full/117/19/4571/DC1). Time elapsed since the beginning of each movie is shown in minutes and seconds; live embryos in this and all other figures are ~50 μm long. Note enrichment at nuclear periphery during prophase (A, time 01:55 and 03:50; B, time 00:00 and 02:15), entry in pronuclei/nuclei during late prophase (A, time 03:50; B, time 02:15), as well as further enrichment in the vicinity of chromosomes during prometaphase (A, time 05:40; not visible in B due to orientation of spindle in ABa and ABp). (C) Quantification of average pixel intensities in the nucleus and a comparable area in the cytoplasm of the four-cell-stage embryo displayed in panel B; results are shown for the time interval between the moment GFP–LIS-1 enrichment becomes apparent at the nuclear periphery and NEBD. Similar plots were obtained in three other embryos. (D,E) FRAP experiments. Images from representative confocal time-lapse sequences of four-cell-stage embryos derived from homozygous *lis-1(1550)* adults expressing GFP–LIS-1 (D) or wild-type animals injected with FITC-labelled Dextran 70 kDa (D) (see also corresponding Movies 11 and 12, in supplementary material). Time elapsed is shown in minutes and seconds. Photobleaching of a ~4.5 μm^2 square (indicated in white) started at time –00:02 and ended at time 00:00. Note very rapid recovery ($t_{1/2}$ ~10 seconds) of fluorescence for both embryos.

GFP–LIS-1 is freely diffusible in the cytoplasm. We investigated whether this is the case using fluorescence recovery after photobleaching (FRAP). We found that photobleaching of GFP–LIS-1 in the cytoplasm is followed by very rapid recovery of fluorescence ($t_{1/2}$ ~10 seconds; Fig. 4D; Movie 11, in supplementary material). An analogous behaviour is observed with fluorescently labelled Dextran of similar size (70 kDa) (Fig. 4E; Movie 12, in supplementary material), compatible with the view that the bulk of LIS-1 is indeed freely diffusible.

LIS-1 is present at kinetochores in a microtubule-independent manner

We next used imaging at the spinning-disc confocal microscope to investigate whether the enrichment in the vicinity of chromosomes during prometaphase reflects interaction with kinetochores. Two non-redundant pathways are required for kinetochore function in *C. elegans* (Oegema et al., 2001); we inactivated each one in turn using RNAi. We found that, whereas inactivation of the INCENP homologue *icp-1* does not alter GFP–LIS-1 distribution (Fig. 5B; Movie 13, in supplementary material, http://jcs.biologists.org/cgi/content/full/117/19/4571/DC1), that of the CENP-C homologue *hcp-4* abolishes GFP–LIS-1 enrichment along chromosomes during prometaphase (Fig. 5C; Movie 14, in supplementary material). Conversely, we found that the kinetochore localization of ICP-1, HCP-4, as well as that of BUB-1, is not affected in the absence of *lis-1* or *dhc*-1 function (Fig. S1, in supplementary material). Overall, we conclude that LIS-1 is present at kinetochores in an *hcp-4*-dependent manner.

To test whether the discrete subcellular distributions of LIS-1, including its presence at kinetochores, require an intact microtubule cytoskeleton, we examined the localization of GFP–LIS-1 in *tba-2(RNAi)* embryos. This probably inactivates all α-tubulin genes owing to cross-RNAi between highly related sequences (Wright and Hunter, 2003). Microtubules are usually undetectable in the resulting one-cell-stage embryos, except for two closely apposed centrosomes located at the very posterior (Fig. 6A,B). We found that GFP–LIS-1 in *tba-2(RNAi)* is not present within pronuclei (Fig. 6A) or in aberrant nuclei of later-stage embryos (Fig. 6D,E). However, GFP–LIS-1 still accumulates at the cell cortex (Fig. 6D, arrow) and at the nuclear periphery (Fig. 6E, arrow) to levels that exceed those

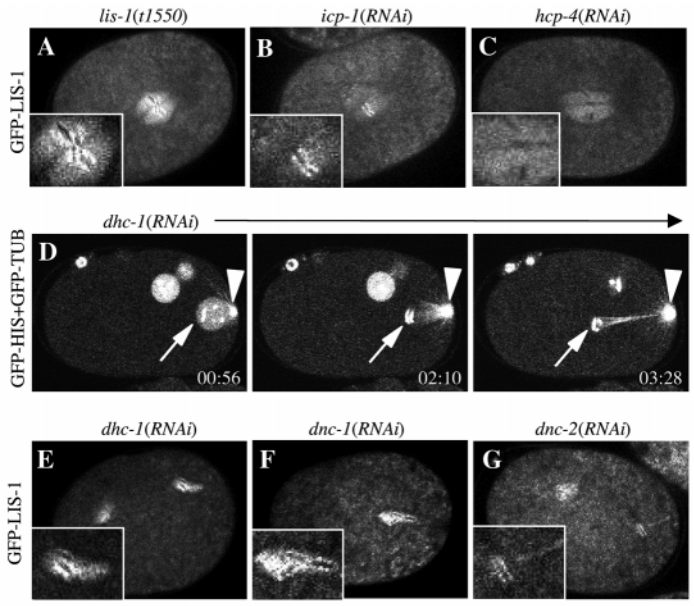

Fig. 5. GFP–LIS-1 localizes to kinetochores independently of dynein. (A-C,E-G) Spinning-disc confocal time-lapse fluorescence microscopy of one-cell-stage embryos derived from homozygous *lis-1(1550)* adults expressing GFP–LIS-1 with no further treatment (A), after *icp-1*(*RNAi*) (B), *hcp-4*(*RNAi*) (C), *dhc-1*(*RNAi*) (E), *dnc-1*(*RNAi*) (F) or *dnc-2*(*RNAi*) (G). A single image during late prometaphase or equivalent stage is shown here; see also corresponding Movies 9, 13, 14, 17, 18 and 19 (in supplementary material, http://jcs.biologists.org/cgi/content/full/117/19/4571/DC1). Insets show ~2.5-fold digitally magnified views of the region encompassing chromosomes. Note that enrichment in the vicinity of chromosomes during prometaphase is absent in *hcp-4*(*RNAi*) embryos (C), but is present in all other cases. Six to twelve embryos were imaged for each genotype, with a similar outcome. (D) Images from confocal time-lapse fluorescence microscopy of *dhc-1*(*RNAi*) one-cell-stage embryo expressing GFP-TUB and GFP-HIS (see also corresponding Movie 16, in supplementary material). Time elapsed is shown in minutes and seconds. Arrows indicate position of chromosomes derived from the male pronucleus. Arrowheads point to the single centrosome visible in this focal plane.

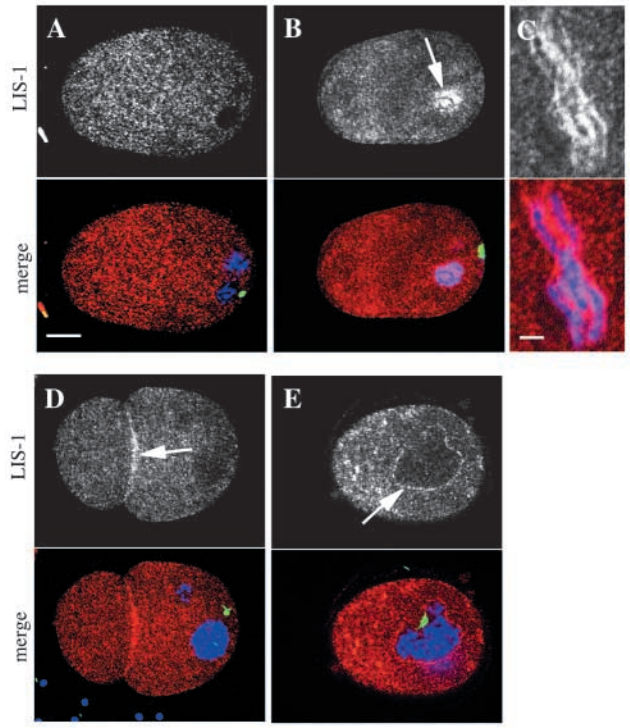

Fig. 6. LIS-1 targeting to the cell cortex, the nuclear periphery and kinetochores is microtubule-independent. Wild-type (C) or *lis-1*(*1550*) embryos rescued by GFP–LIS-1 expression (A,B,D,E) treated with *tba-2* (*RNAi*) and stained with antibodies against LIS-1 and α-tubulin; upper panels show LIS-1 staining, lower panels the merge of LIS-1 (red), α-tubulin (green), and Hoechst counterstain to view DNA (blue). (A) One-cell-stage embryo prior to pronuclear envelope breakdown; note that GFP–LIS-1 is excluded from pronuclei. (B) One-cell-stage embryo during mitosis; note intense GFP–LIS-1 in the vicinity of condensed chromosomes (arrow). (C) High magnification view of chromosomes in an embryo at a later cell cycle. Embryo posterior is up; bar, 2 μm. Note that LIS-1 enrichment follows the position of chromosomes. (D) Embryo at a later cell cycle; note cortical enrichment of GFP–LIS-1 (arrow). (E) Later-stage embryo during prophase; note enrichment at the nuclear periphery (arrow). Images are projections of up to three consecutive 1 μm confocal slices.

observed in the wild-type (compare with Fig. 3). Identical results were observed for LIS-1 localization in wild-type embryos treated with *tba-2(RNAi)* (data not shown). Furthermore, we found that GFP–LIS-1 and LIS-1 are still enriched along prometaphase chromosomes in *tba-2(RNAi)* embryos (Fig. 6B, arrow; 6C),as confirmed by imaging GFP–LIS-1 in *tba-2(RNAi)* embryos at the spinning-disc confocal microscope (Movie 15, in supplementary material). Together, these findings establish that microtubules are dispensable for LIS-1 enrichment at the nuclear periphery, the cell cortex and kinetochores.

Reciprocal relationship of *dhc-1* and *lis-1*

Although LIS-1 localization resembles that of DHC-1, there are also differences; for instance, DHC-1 is not detected in the nucleus prior to NEBD (Gönczy et al., 1999a). Double labelling of GFP–LIS-1-transgenic embryos with DHC-1 and GFP antibodies confirmed that LIS-1 is already nuclear when DHC-1 is merely present at the nuclear periphery (Fig. 7A). Furthermore, we observed that many cytoplasmic foci of DHC-1 and GFP–LIS-1 do not appear to colocalize (Fig. 7B), suggesting that not all DHC-1 and LIS-1 are complexed at any one time.

We next tested whether the discrete subcellular distributions of DHC-1 depend on *lis-1* function. In wild-type embryos, DHC-1 is enriched at the cell cortex, in the vicinity of microtubule asters, at the nuclear periphery and at kinetochores (Gönczy et al., 1999a). We found that DHC-1 distribution at kinetochores in the wild-type is too weak to ascertain reliably whether it is affected when *lis-1* function is compromised (data not shown). By contrast, we discovered that DHC-1 enrichment at the cell cortex, the vicinity of microtubule asters and the nuclear periphery is less pronounced in *lis-1(t1550)* embryos than in the wild-type (Fig. 7D, compare with 7C). We conclude that *lis-1* contributes to, but does not appear to be essential for, targeting DHC-1 to these specific subcellular locations.

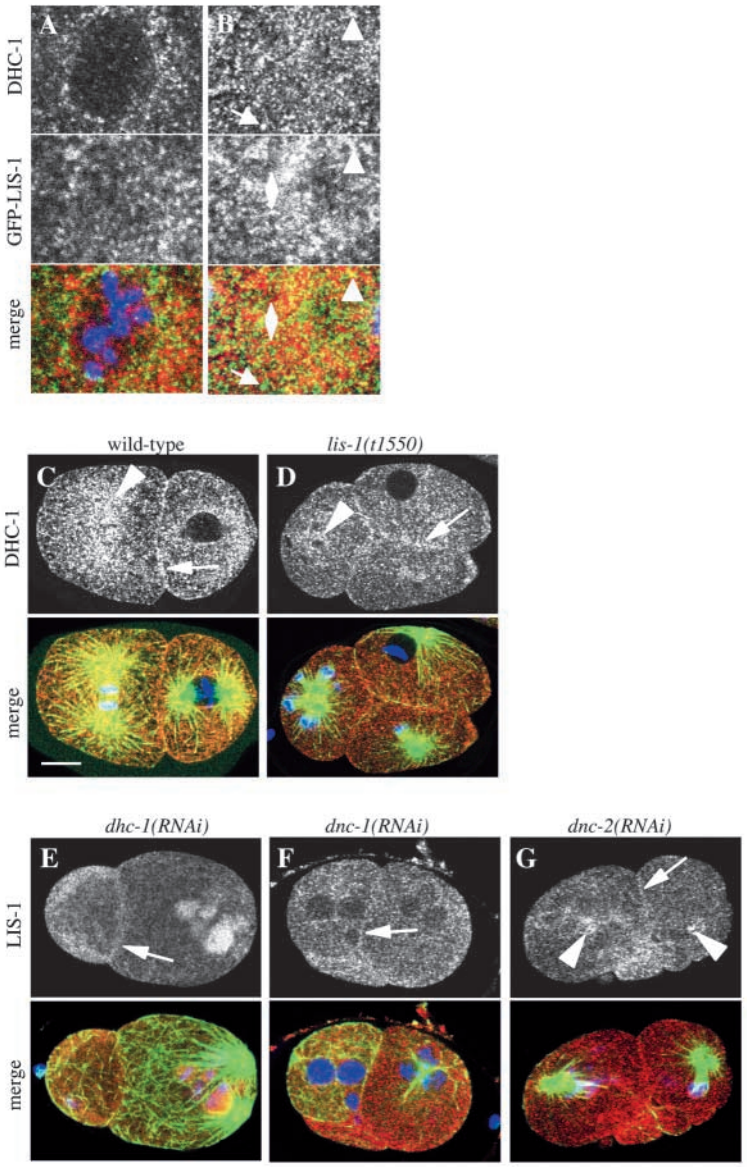

Fig. 7. Relationship between *lis-1* and dynein/dynactin. (A,B) Embryo at the two-to-four cell stage transition expressing GFP–LIS-1 and stained with antibodies against DHC-1 and GFP; upper panels shows DHC-1, middle panel shows GFP, lower panel the merge of GFP (red), DHC-1 (green), and Hoechst counterstain to view DNA (blue). Panel A (approximately 6×10 μm) shows high magnification of the P_1 nucleus during late prophase, panel B (approximately 3×5 μm) a cytoplasmic area from the AB cell in the same embryo. Bottom of diamond points to a focus of GFP–LIS-1 that does not coincide with intense DHC-1 staining, arrow to a focus of DHC-1 that does not coincide with intense GFP–LIS-1 staining, arrowhead to a focus of coincident DHC-1 and GFP–LIS-1 staining. (C,D) Wild-type (C) and *lis-1*(*t1550*) (D) two-cell-stage-equivalent embryos stained with antibodies against DHC-1 and α-tubulin. Upper panels show DHC-1 staining, lower panels the merge of DHC-1(red), α-tubulin (green) and Hoechst counterstain to view DNA (blue). Note that DHC-1 enrichment at the nuclear periphery, in the vicinity of microtubule asters (arrowheads) and at the cell cortex (arrows) are all somewhat diminished in *lis-1*(*t1550*) mutant embryos compared with wild-type. In rare *lis-1(t1550)* embryos, enrichment of DHC-1 at specific subcellular locations appeared to be absent (not shown). Bar, 10 μm. (E-G) *dhc-1*(*RNAi*) (E), *dnc-1*(*RNAi*) (F) or *dnc-2*(*RNAi*) (G) embryos at the second cell cycle stained with antibodies against LIS-1 and α-tubulin. Upper panels show anti-LIS-1 staining, lower panel the merge of LIS-1(red), α-tubulin (green) and Hoechst counterstain to view DNA (blue). Note that LIS-1 is still present at the cell cortex (arrows), albeit to somewhat lower levels than in the wild-type (compare with Fig. 3D). Note also that LIS-1 enrichment along chromosomes is visible in the *dnc-2*(*RNAi*) embryo (G, arrowhead). Moreover, note that LIS-1 becomes trapped in nuclear compartments after the first failed cell division in this particular *dhc-1*(*RNAi*) embryo (E); this was not observed in all *dhc-1*(*RNAi*) embryos examined, and only rarely after inactivation of dynactin components.

Conversely, we addressed whether the discrete subcellular distributions of LIS-1 depend on *dhc-1*, *dnc-1* and *dnc-2* function. Analysis of fixed specimens showed that enrichment of LIS-1 at the cell cortex is somewhat diminished compared with wild-type in *dhc-1*(*RNAi*), *dnc-1*(*RNAi*) and *dnc-2*(*RNAi*) embryos (Fig. 7E-G, arrows, compare with Fig. 3D). We also noted that LIS-1 sometimes remains present in the nuclear compartments formed after the failed first cell division in *dhc-1*(*RNAi*) embryos (Fig. 7E).

We set out to conduct live imaging of GFP–LIS-1 to test whether distribution at kinetochores and at the nuclear periphery is altered when dynein or dynactin function is compromised. To characterize better the location of chromosomes in such embryos, we first imaged *dhc-1*(*RNAi*) embryos expressing GFP-TUB and GFP-HIS (Movie 16, in supplementary material, http://jcs.biologists.org/cgi/content/full/117/19/4571/DC1). This revealed that, following breakdown of the male pronucleus, microtubules emanating from the two centrosomes appear to 'push' chromosomes towards the anterior (Fig. 5D). These microtubules presumably correspond to the yolk-granule-depleted region observed in embryos with compromised *dhc-1* or *lis-1* function (Fig. 2B,C, arrows) (Gönczy et al., 1999a).

Importantly, imaging at the spinning-disc confocal established that GFP–LIS-1 is enriched along chromosomes being 'pushed' towards the anterior in *dhc-1*(*RNAi*), *dnc-1*(*RNAi*) and *dnc-2*(*RNAi*) embryos (Fig. 5E-G), in a manner analogous to the enrichment observed in the wild-type at this stage (Fig. 5A). In stark contrast, we found that enrichment of GFP–LIS-1 at the nuclear periphery is absent in *dhc-1*(*RNAi*), *dnc-1*(*RNAi*) and *dnc-2*(*RNAi*) embryos (Movies 17-19, in supplementary material).

Taken together, these findings lead us to conclude that *dhc-1*, *dnc-1* and *dnc-2* contribute to LIS-1 enrichment at the cell cortex, appear dispensable for its presence at kinetochores, but are essential for LIS-1 targeting to the nuclear periphery.

Discussion

C. elegans embryos have identical requirements for *lis-1* and dynein

Our work establishes using loss-of-function analysis in a metazoan organism that Lis1 is required for all known dynein-dependent processes in a given cell. Previous suggestions that Lis1 might not serve as an obligate cofactor for dynein function were inferred from overexpression experiments, whose interpretation can be complicated by dominant-negative effects. In fact, two such studies reached different conclusions regarding whether localization of the Golgi apparatus, which is a dynein-dependent process, is perturbed by Lis1 overexpression (Faulkner et al., 2000; Smith et al., 2000). The two likely null mutant alleles described here set the stage for a comprehensive genetic dissection of a Lis1 family member in a metazoan organism. This will be particularly interesting given that many of the components that physically interact with Lis1 in other systems (reviewed by Caspi et al., 2003; Morris et al., 1998; Reiner, 2000; Wynshaw-Boris and Gambello, 2001) are present in *C. elegans*, thus permitting an investigation of the functional significance of these interactions in vivo.

Whereas patients lacking one functional copy of Lis1 have severe neurological disorders, loss of both copies of the gene is probably incompatible with human life. Accordingly, inactivation of both copies of Lis1 results in early embryonic lethality in the mouse, as it does in *Drosophila* (Hirotsune et al., 1998; Liu et al., 1999; Swan et al., 1999). By contrast, we found that *C. elegans lis-1*, although being required maternally, is largely dispensable zygotically, as most homozygous mutant animals survive to become fertile adults (Materials and Methods). One likely explanation is that maternally contributed LIS-1 can carry out most functions that are essential for viability during embryonic and post-embryonic development. Similarly, in the mouse, maternally contributed protein might ensure function during the first few cell cycles, as death of homozygous mutant embryos coincides with zygotic transcription (Cahana et al., 2003).

In *C. elegans*, it remains to be determined whether *lis-1*(*t1550*) or *lis-1*(*t1698*) homozygous mutant animals have a neuronal phenotype. Compatible with a potential role for *lis-1* in neurons, a *lis-1* promoter reporter is expressed in larval neuronal lineages (Dawe et al., 2001), as is LIS-1 protein (M.M.C. and P.G., unpublished). Furthermore, animals that escape the embryonic lethality conferred by *lis-1*(*RNAi*) become uncoordinated adults (Dawe et al., 2001). Therefore, the two mutant alleles described here should also prove extremely valuable for undertaking a genetic analysis of the requirement for *lis-1* function in neurons.

LIS-1 localizes to microtubules, but not strictly to their plus ends

It has been suggested that Lis1 plays an important role at microtubule plus ends to mediate interactions with the cell cortex (reviewed by Dujardin and Vallee, 2002). In *C. elegans*, we found that whereas LIS-1 colocalizes with microtubules, it is not significantly enriched at plus ends as compared with more internal parts of the lattice. Moreover, we found that LIS-1 localizes along the entire length of microtubules upon cold treatment followed by short periods of regrowth (M.M.C. and P.G., unpublished), indicating that LIS-1 does not preferentially recognize growing microtubules. In mammalian cells, Lis1 is also observed throughout microtubule-dense regions (Aumais et al., 2001; Smith et al., 2000). Such even distributions along microtubules are in contrast to the striking plus-end enrichment observed for *S. cerevisiae* Pac1p or *A. nidulans* NudF (Han et al., 2001; Lee et al., 2003). The difference might reflect distinct equilibrium distributions of motor complexes in fungi, where dynein has few biological roles, and metazoan organisms, where it has many. Overall, our findings strengthen the notion that, in contrast to plus tip components such as CLIP-170 (Perez et al., 1999; Schuyler and Pellman, 2001), Lis1-family members do not exclusively recognize structural features at the plus end of microtubules.

Microtubules are dispensable for localization of DLis-1 to the oocyte cortex in *Drosophila* (Swan et al., 1999). Similarly, we find that microtubules are not required for the presence of LIS-1 on the nuclear envelope, at the cell cortex or at kinetochores in *C. elegans*. In fact, we found that LIS-1 enrichment at these specific subcellular locations appears greater in *tba-2*(*RNAi*) embryos, raising the possibility that microtubules negatively regulate the targeting of Lis1 proteins. In agreement with this model, the localization of Lis1 to the nuclear periphery of some mammalian cells is apparent only when microtubules are depolymerized (Smith et al., 2000).

Reciprocal relationship of *dhc-1* and *lis-1*

Our analysis using loss-of-function conditions contributes to clarifying the relationship between Lis1 and the dynein/dynactin-family members in metazoan organisms. We found that *lis-1* function is required for efficient DHC-1 enrichment at the cell cortex, in the vicinity of microtubule asters and at the nuclear periphery. In *Drosophila* oocytes, DLis-1 is essential for accumulation of dynein at the cell cortex (Swan et al., 1999). Similarly, *S. cerevisiae* Pac1p is required for the localization of the dynein heavy chain Dyn1p, in this case to microtubule plus ends (Lee et al., 2003; Sheeman et al., 2003). Whereas our findings are in line with these studies, they also indicate that components other than *lis-1* contribute to efficient targeting of dynein in *C. elegans* embryos, since some DHC-1 enrichment remains in probable null *lis-1* mutants.

We also found that *dhc-1*, *dnc-1* and *dnc-2* are essential for LIS-1 localization at the nuclear periphery. By contrast, all three genes appear to be largely dispensable for LIS-1 enrichment at the cell cortex, and entirely dispensable for its enrichment at kinetochores. On the basis of overexpression studies in COS-7 and HeLa cells (Coquelle et al., 2002; Tai et al., 2002), it has been proposed that dynein and dynactin recruit Lis1 to kinetochores. Our data suggest that Lis1 targeting to kinetochores can occur independently of either dynein or dynactin activity. Alternatively, Lis1 could be targeted to kinetochores redundantly through dynein and dynactin as we did not examine LIS-1 distribution in embryos simultaneously inactivated for *dhc-1* and a dynactin component. As a fraction of dynein in other systems localizes to kinetochores independently of microtubules (King et al., 2000), our findings also raise the possibility that kinetochore-associated dynein is targeted there by Lis1 proteins. Elucidating the detailed mechanisms by which Lis1 and dynein present at kinetochores

and other subcellular locations govern cell division processes is an important challenge for future studies.

We are grateful to M. Delattre, K. Afshar and V. Simanis for critical reading of the manuscript. We thank M. Glotzer, J. Beaudouin, J. Ellenberg, K. Oegema and V. Simanis for reagents. Supported by a Roche Research Foundation fellowship (2001-88 to M.C.), ISREC and a grant from the Swiss National Science Foundation (31-62102.00 to P.G.).

References

Aumais, J. P., Tunstead, J. R., McNeil, R. S., Schaar, B. T., McConnell, S. K., Lin, S. H., Clark, G. D. and Yu-Lee, L. Y. (2001). NudC associates with Lis1 and the dynein motor at the leading pole of neurons. *J. Neurosci.* **21**, RC187.

Beaudouin, J., Gerlich, D., Daigle, N., Eils, R. and Ellenberg, J. (2002). Nuclear envelope breakdown proceeds by microtubule-induced tearing of the lamina. *Cell* **108**, 83-96.

Bellanger, J. M. and Gönczy, P. (2003). TAC-1 and ZYG-9 form a complex that promotes microtubule assembly in *C. elegans* embryos. *Curr. Biol.* **13**, 1488-1498.

Brenner, S. (1974). The genetics of *Caenorhabditis elegans*. *Genetics* **77**, 71-94.

Busson, S., Dujardin, D., Moreau, A., Dompierre, J. and de Mey, J. R. (1998). Dynein and dynactin are localized to astral microtubules and at cortical sites in mitotic epithelial cells. *Curr. Biol.* **8**, 541-544.

Cahana, A., Jin, X. L., Reiner, O., Wynshaw-Boris, A. and O'Neill, C. (2003). A study of the nature of embryonic lethality in LIS1$^{-/-}$ mice. *Mol. Reprod. Dev.* **66**, 134-142.

Caspi, M., Coquelle, F. M., Koifman, C., Levy, T., Arai, H., Aoki, J., de Mey, J. R. and Reiner, O. (2003). LIS1 missense mutations, variable phenotypes result from unpredictable alterations in biochemical and cellular properties. *J. Biol. Chem.* **278**, 38740-38748.

Coquelle, F. M., Caspi, M., Cordelieres, F. P., Dompierre, J. P., Dujardin, D. L., Koifman, C., Martin, P., Hoogenraad, C. C., Akhmanova, A., Galjart, N. et al. (2002). LIS1, CLIP-170's key to the dynein/dynactin pathway. *Mol. Cell. Biol.* **22**, 3089-3102.

Culbertson, M. R. and Leeds, P. F. (2003). Looking at mRNA decay pathways through the window of molecular evolution. *Curr. Opin. Genet. Dev.* **13**, 207-214.

Dawe, A. L., Caldwell, K. A., Harris, P. M., Morris, N. R. and Caldwell, G. A. (2001). Evolutionarily conserved nuclear migration genes required for early embryonic development in *Caenorhabditis elegans*. *Dev. Genes Evol.* **211**, 434-441.

Dechant, R. and Glotzer, M. (2003). Centrosome separation and central spindle assembly act in redundant pathways that regulate microtubule density and trigger cleavage furrow formation. *Dev. Cell* **4**, 333-344.

Dujardin, D. L. and Vallee, R. B. (2002). Dynein at the cortex. *Curr. Opin. Cell Biol.* **14**, 44-49.

Faulkner, N. E., Dujardin, D. L., Tai, C. Y., Vaughan, K. T., O'Connell, C. B., Wang, Y. and Vallee, R. B. (2000). A role for the lissencephaly gene LIS1 in mitosis and cytoplasmic dynein function. *Nat. Cell Biol.* **2**, 784-791.

Gambello, M. J., Darling, D. L., Yingling, J., Tanaka, T., Gleeson, J. G. and Wynshaw-Boris, A. (2003). Multiple dose-dependent effects of Lis1 on cerebral cortical development. *J. Neurosci.* **23**, 1719-1729.

Geiser, J. R., Schott, E. J., Kingsbury, T. J., Cole, N. B., Totis, L. J., Bhattacharyya, G., He, L. and Hoyt, M. A. (1997). *Saccharomyces cerevisiae* genes required in the absence of the CIN8-encoded spindle motor act in functionally diverse mitotic pathways. *Mol. Biol. Cell* **8**, 1035-1050.

Gill, S. R., Schroer, T. A., Szilak, I., Steuer, E. R., Sheetz, M. P. and Cleveland, D. W. (1991). Dynactin, a conserved, ubiquitously expressed component of an activator of vesicle motility mediated by cytoplasmic dynein. *J. Cell Biol.* **115**, 1639-1650.

Gönczy, P. (2002). Mechanisms of spindle positioning, focus on flies and worms. *Trends Cell Biol.* **12**, 332-339.

Gönczy, P., Pichler, S., Kirkham, M. and Hyman, A. A. (1999a). Cytoplasmic dynein is required for distinct aspects of MTOC positioning, including centrosome separation, in the one cell stage *Caenorhabditis elegans* embryo. *J. Cell Biol.* **147**, 135-150.

Gönczy, P., Schnabel, H., Kaletta, T., Amores, A. D., Hyman, T. and Schnabel, R. (1999b). Dissection of cell division processes in the one cell stage *Caenorhabditis elegans* embryo by mutational analysis. *J. Cell Biol.* **144**, 927-946.

Gönczy, P., Echeverri, C., Oegema, K., Coulson, A., Jones, S. J., Copley, R. R., Duperon, J., Oegema, J., Brehm, M., Cassin, E. et al. (2000). Functional genomic analysis of cell division in *C. elegans* using RNAi of genes on chromosome III. *Nature* **408**, 331-336.

Gönczy, P., Bellanger, J. M., Kirkham, M., Pozniakowski, A., Baumer, K., Phillips, J. B. and Hyman, A. A. (2001). *zyg-8*, a gene required for spindle positioning in *C. elegans*, encodes a doublecortin-related kinase that promotes microtubule assembly. *Dev. Cell* **1**, 363-375.

Han, G., Liu, B., Zhang, J., Zuo, W., Morris, N. R. and Xiang, X. (2001). The *Aspergillus* cytoplasmic dynein heavy chain and NUDF localize to microtubule ends and affect microtubule dynamics. *Curr. Biol.* **11**, 719-724.

Hattori, M., Adachi, H., Tsujimoto, M., Arai, H. and Inoue, K. (1994). Miller-Dieker lissencephaly gene encodes a subunit of brain platelet-activating factor acetylhydrolase. *Nature* **370**, 216-218.

Hirotsune, S., Fleck, M. W., Gambello, M. J., Bix, G. J., Chen, A., Clark, G. D., Ledbetter, D. H., McBain, C. J. and Wynshaw-Boris, A. (1998). Graded reduction of Pafah1b1 (Lis1) activity results in neuronal migration defects and early embryonic lethality. *Nat. Genet.* **19**, 333-339.

Holzbaur, E. L. and Vallee, R. B. (1994). DYNEINS, molecular structure and cellular function. *Annu. Rev. Cell Biol.* **10**, 339-372.

Kamath, R. S., Martinez-Campos, M., Zipperlen, P., Fraser, A. G. and Ahringer, J. (2001). Effectiveness of specific RNA-mediated interference through ingested double-stranded RNA in *Caenorhabditis elegans*. *Genome Biol.* **2**, research0002.1-research0002.10.

Karki, S. and Holzbaur, E. L. (1999). Cytoplasmic dynein and dynactin in cell division and intracellular transport. *Curr. Opin. Cell Biol.* **11**, 45-53.

King, J. M., Hays, T. S. and Nicklas, R. B. (2000). Dynein is a transient kinetochore component whose binding is regulated by microtubule attachment, not tension. *J. Cell Biol.* **151**, 739-748.

Lee, W. L., Oberle, J. R. and Cooper, J. A. (2003). The role of the lissencephaly protein Pac1 during nuclear migration in budding yeast. *J. Cell Biol.* **160**, 355-364.

Lin, S. X. and Collins, C. A. (1992). Immunolocalization of cytoplasmic dynein to lysosomes in cultured cells. *J. Cell Sci.* **101**, 125-137.

Liu, Z., Xie, T. and Steward, R. (1999). Lis1, the *Drosophila* homolog of a human lissencephaly disease gene, is required for germline cell division and oocyte differentiation. *Development* **126**, 4477-4488.

Matthews, L. R., Carter, P., Thierry-Mieg, D. and Kemphues, K. (1998). ZYG-9, a *Caenorhabditis elegans* protein required for microtubule organization and function, is a component of meiotic and mitotic spindle poles. *J. Cell Biol.* **141**, 1159-1168.

Morris, N. R., Efimov, V. P. and Xiang, X. (1998). Nuclear migration, nucleokinesis and lissencephaly. *Trends Cell Biol.* **8**, 467-470.

Oegema, K., Desai, A., Rybina, S., Kirkham, M. and Hyman, A. A. (2001). Functional analysis of kinetochore assembly in *Caenorhabditis elegans*. *J. Cell Biol.* **153**, 1209-1226.

Perez, F., Diamantopoulos, G. S., Stalder, R. and Kreis, T. E. (1999). CLIP-170 highlights growing microtubule ends in vivo. *Cell* **96**, 517-527.

Pfarr, C. M., Coue, M., Grissom, P. M., Hays, T. S., Porter, M. E. and McIntosh, J. R. (1990). Cytoplasmic dynein is localized to kinetochores during mitosis. *Nature* **345**, 263-265.

Praitis, V., Casey, E., Collar, D. and Austin, J. (2001). Creation of low-copy integrated transgenic lines in *Caenorhabditis elegans*. *Genetics* **157**, 1217-1226.

Reiner, O. (2000). LIS1. Let's interact sometimes... (part 1). *Neuron* **28**, 633-636.

Reiner, O., Carrozzo, R., Shen, Y., Wehnert, M., Faustinella, F., Dobyns, W. B., Caskey, C. T. and Ledbetter, D. H. (1993). Isolation of a Miller-Dieker lissencephaly gene containing G protein beta-subunit-like repeats. *Nature* **364**, 717-721.

Salina, D., Bodoor, K., Eckley, D. M., Schroer, T. A., Rattner, J. B. and Burke, B. (2002). Cytoplasmic dynein as a facilitator of nuclear envelope breakdown. *Cell* **108**, 97-107.

Savoian, M. S., Goldberg, M. L. and Rieder, C. L. (2000). The rate of poleward chromosome motion is attenuated in *Drosophila* zw10 and rod mutants. *Nat. Cell Biol.* **2**, 948-952.

Schuyler, S. C. and Pellman, D. (2001). Microtubule 'plus-end-tracking proteins', the end is just the beginning. *Cell* **105**, 421-424.

Sharp, D. J., Rogers, G. C. and Scholey, J. M. (2000). Cytoplasmic dynein is required for poleward chromosome movement during mitosis in *Drosophila* embryos. *Nat. Cell Biol.* **2**, 922-930.

Sheeman, B., Carvalho, P., Sagot, I., Geiser, J., Kho, D., Hoyt, M. A. and Pellman, D. (2003). Determinants of *S. cerevisiae* Dynein localization and activation. Implications for the mechanism of spindle positioning. *Curr. Biol.* **13**, 364-372.

Smith, D. S., Niethammer, M., Ayala, R., Zhou, Y., Gambello, M. J., Wynshaw-Boris, A. and Tsai, L. H. (2000). Regulation of cytoplasmic dynein behaviour and microtubule organization by mammalian Lis1. *Nat. Cell Biol.* **2**, 767-775.

Steuer, E. R., Wordeman, L., Schroer, T. A. and Sheetz, M. P. (1990). Localization of cytoplasmic dynein to mitotic spindles and kinetochores. *Nature* **345**, 266-268.

Strome, S., Powers, J., Dunn, M., Reese, K., Malone, C. J., White, J., Seydoux, G. and Saxton, W. (2001). Spindle dynamics and the role of gamma-tubulin in early *Caenorhabditis elegans* embryos. *Mol. Biol. Cell* **12**, 1751-1764.

Swan, A., Nguyen, T. and Suter, B. (1999). *Drosophila* Lissencephaly-1 functions with Bic-D and dynein in oocyte determination and nuclear positioning. *Nat. Cell Biol.* **1**, 444-449.

Tai, C. Y., Dujardin, D. L., Faulkner, N. E. and Vallee, R. B. (2002). Role of dynein, dynactin, and CLIP-170 interactions in LIS1 kinetochore function. *J. Cell Biol.* **156**, 959-968.

Timmons, L., Court, D. L. and Fire, A. (2001). Ingestion of bacterially expressed dsRNAs can produce specific and potent genetic interference in *Caenorhabditis elegans*. *Gene* **263**, 103-112.

Vaisberg, E. A., Koonce, M. P. and McIntosh, J. R. (1993). Cytoplasmic dynein plays a role in mammalian mitotic spindle formation. *J. Cell Biol.* **123**, 849-858.

Vale, R. D. (2003). The molecular motor toolbox for intracellular transport. *Cell* **112**, 467-480.

Wright, A. J. and Hunter, C. P. (2003). Mutations in a beta-tubulin disrupt spindle orientation and microtubule dynamics in the early *Caenorhabditis elegans* embryo. *Mol. Biol. Cell* **11**, 4512-4525.

Wynshaw-Boris, A. and Gambello, M. J. (2001). LIS1 and dynein motor function in neuronal migration and development. *Genes Dev.* **15**, 639-651.

Xiang, X. (2003). LIS1 at the microtubule plus end and its role in dynein-mediated nuclear migration. *J. Cell Biol.* **160**, 289-290.